COMBINED NUMERICAL FINITE ELEMENT AND EXPERIMENTAL OPTIMIZATION APPROACH IN THE PRODUCTION PROCESS OF MEDIUM-VOLTAGE, RUBBER-INSULATED ELECTRIC CABLES VULCANIZED WITH STEAM WATER. PART 2: NUMERICAL SIMULATIONS AND INVERSE ANALYSES

G. MILANI,[1,*] F. MILANI[2]

[1]TECHNICAL UNIVERSITY OF MILAN, PIAZZA LEONARDO DA VINCI 32, 20133, MILAN, ITALY
[2]CHEM.CO CONSULTANT, VIA J. F. KENNEDY 2, 45030 OCCHIOBELLO, ROVIGO, ITALY

INTRODUCTION

In the accompanying paper, Part 1, an actual production line, 103 m long, was analyzed experimentally. The differential scanning calorimetry (DSC) results showed that, at four different vulcanization conditions with steam, the resulting degree of reticulation at the end of the production process was sensibly lower than that expected from the simplified evaluations based on the knowledge of the half-life of the peroxides used, especially when the steam temperature was low and the exposure time was reduced. The situation was critical in the internal layers.

The present article, Part 2, is aimed at analyzing the vulcanization process numerically, trying to identify the reasons at the base of such an unexpected undervulcanization of the cable. The finite element analysis of the heat-transfer process during rubber vulcanization has a long tradition and has been successfully applied by many authors to predict the degree of reticulation at the end of several different production processes.[1–10] However, when an experimental characterization of the cure level at the end of the industrial process is available, as in the present case, it is interesting to perform numerical back-analyses to determine the values of some of the input parameters linked to a minimization of the output error when compared with experimental evidence. Within that framework, the combined approach proposed in the present article may be regarded as innovative and beneficial for producers interested in a quantitative evaluation of the level of cure obtained during the production process.

*Corresponding author. Ph: +39-02-2399-4290; email: gabriele.milani@polimi.it

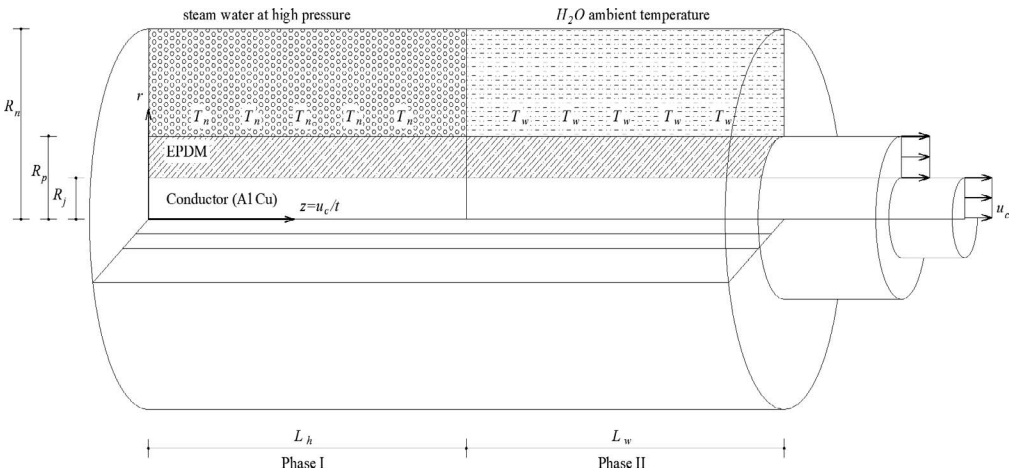

FIG. 1. — Schematic representation of the heating (phase I) and cooling (phase II) phases with water.

Optimization of the input parameters was performed with an inverse analysis of a nonstandard, meta-heuristic approach, based on genetic algorithm (GA) concepts. Rather than using gradient-based routines with standard least-squares minimization of experimental data, this process is appealing because the cross-linking density at the end of the industrial process is not known analytically.

At fixed input parameters, the determination of the level of curing is typically obtained by finite element (FE) simulations. When FEs were used to determine the degree of cross-linking of the cable under a constant vulcanization temperature, a partial match between the numeric predictions and experimental evidence from the DSC was found, indicating a clear discrepancy between the set parameters and the real values. Such results suggest that the steam-curing temperature along the pipe length probably decreased and that one of the key input parameters to optimize the GA process is the steam temperature variable.

GA parameters are the temperatures at different positions of the pipe, and the objective (fitness) function is represented by the sum of the squared difference between the numeric predictions and the experimental determination of the degree of cross-linking. The proposed GA is robust and nonstandard and is based on a specifically developed, zooming strategy, which is composed of a subdivision of the population at each iteration into two subgroups that depend on individual's fitness grade (the elitist strategy). Different genetic procedures were applied to the subgroups, namely, the two typologies of admissible mutations for the elite subpopulation and the mutation and reproduction for the remaining individuals. To improve the algorithm convergence, a user-defined population percentage that depends on an individual's fitness was replaced with new phenotypes at the end of each iteration, thereby enforcing the chromosome renewal.

The aim of the proposed numeric approach is not only to fit the experimental data using least-squares best fit but also to suggest a simple and efficient computational tool that is able to determine the expected level of cross-linking.

GOVERNING PARTIAL-DIFFERENTIAL EQUATIONS

The actual production plant had to be idealized before applying any mathematical model. Therefore, the vulcanization process was schematically subdivided (Figure 1) into two simple phases: (1) the heating zone, and (2) the cooling zone.

Index j indicates the metallic conductor (semidiameter R_j), and index p indicates insulation width (external radius R_p).

The axial symmetry of the cable leads to an independent, two-variables system: the distance r of an insulation layer with respect to the cable axis, and an exposure time t. At a constant cable speed, a cable section at distance z, with respect to the starting point of the production line, is characterized by an exposure time equal to $t = z/u_c$. This means the z variable is dependent on t.

During the heating phase, pressurized steam at the temperature T_n is used, which exchanges heat with the EPDM surface, primarily by convection. Fourier's heat equation for cylindrical coordinates was used to determine the temperature profiles numerically along the thickness of the cable (see ref 5 for details). For the insulation layer, the heat-balance field used the following equation:

$$\rho_p c_p^p \left(\frac{\partial T}{\partial t}\right) - \lambda_p \left(\frac{\partial^2 T}{\partial r^2} + \frac{1}{r}\frac{\partial T}{\partial r}\right) + r_p \Delta H_r = 0 \tag{1}$$

where ρ_p, c_p^p, and λ_p are EPDM density, specific heat capacity, and heat conductivity, respectively; ΔH_r is the insulation specific heat of the reaction expressed in kilojoules per mole; and r_p is the rate of cross-linking expressed in moles per 1 s.

The term $r_p \Delta H_r$ in Eq. 1. is the heat produced by the decomposition of the peroxide. ΔH_r depends both on the type of peroxide used and the type of hydrogen extracted (allylic, vinylic, etc.). For simplicity, we assumed a linear behavior for r_p with respect to concentration, that is, $r_p = dC/dt$.

Similar considerations can be repeated for the conductor, obviously assuming $\Delta H_r = 0$:

$$\rho_j c_j^p \left(\frac{\partial T}{\partial t}\right) - \lambda_j \left(\frac{\partial^2 T}{\partial r^2} + \frac{1}{r}\frac{\partial T}{\partial r}\right) = 0 \tag{2}$$

where the index j refers to the conductor layer.

Because heat equation is of a second order in space, two boundary conditions must be specified. In particular, for the problem at hand, at $r = 0$, a symmetry condition on the temperature field was imposed in the well-known form $(\partial T/\partial r) = 0$, whereas at $r = R_p$, we impose the following equation:

$$\lambda_p \frac{\partial T}{\partial r} + h\big[T(R_p, t) - T_n\big] + q_{rad} = 0 \tag{3}$$

where h is the heat-transfer coefficient between EPDM and the steam, T_n is the steam temperature, and q_{rad} is the heat flux transferred by radiation. Here, for vulcanization with steam, the evaluation of q_{rad} would be a rather difficult task. In fact, the well-known radiation formulas in polar coordinates cannot be applied rigorously because the water vapor participates in the radiation exchange between the tube wall and the insulation surface. Because typical values for the convection coefficient are used for the steam condensation, radiation is not included in the model because of the complexity of accurately including the radiation effects.

Finally, at the interface between the conductor and the insulation, an equilibrium equation on the heat flux exchanged is imposed in the following form: $\lambda_j\{[\partial T(R_j, t)]/\partial r\} = \lambda_p\{[\partial T(R_p, t)]/\partial \mathrm{r}\}$.

For transient conduction, the heat is a first-order equation in time, requiring the assumption of an initial temperature distribution:

$$\begin{aligned} T(r, 0) &= T_j^0 \quad 0 \le r < R_j \\ T(r, 0) &= T_p^0 \quad R_j \le r \le R_p \end{aligned} \tag{4}$$

No differences occur in the cooling zone, except that boundary Eq. 3 is replaced by a pure-convection equation: $\lambda_p(\partial T/\partial r) + h_w[T(R_p, t) - T_w] = 0$, where h_w is the water heat-transfer coefficient, and T_w is the water cooling temperature.

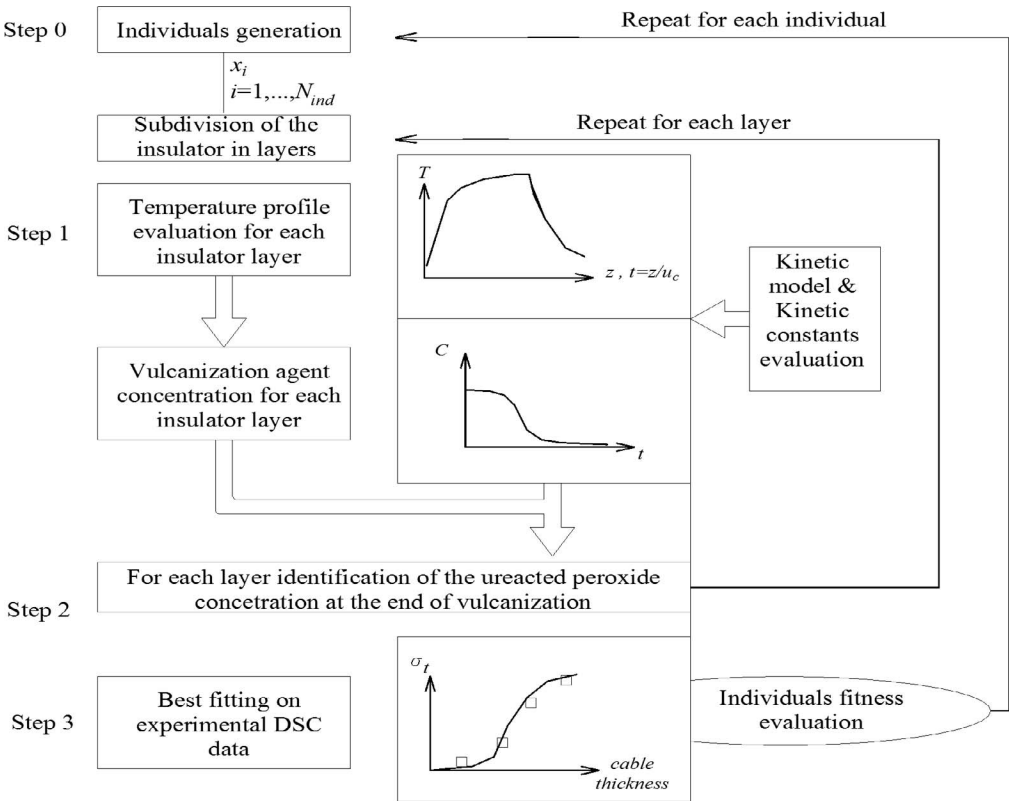

FIG. 2. — Schematic representation of the numeric procedure adopted to eventually determine final tensile strength and cross-link density of each layer.

Initial temperature conditions are obtained from the profile evaluated at the last step of the cooling zone, that is, at $T(r, t_c)$, where $t_c = L_c/u_c$, where L_c is the curing-zone length.

The resulting partial differential equation is solved with a consolidated FE approach under axisymmetric conditions. In the numeric simulations, the following general parameters were used: EPM/EPDM density is $\rho_p = 922$ Kg/m^3; insulation specific heat capacity is $c_p^p = 2700$J/kg °C, $\lambda_p = 0.335$ W/m °C; conductor density is $\rho_j = 2707$ Kg/m^3; conductor specific heat capacity is $c_j^p = 8.96$J/kg °C, $\lambda_j = 300$ W/m °C, ΔH_r kJ/mol; the water heat transfer coefficient is $h_w = 1490.70$ W/m^2 °C; and the steam water heat transfer coefficient is $h = 120$ W/m^2 °C. The value assumed for h is a rough estimate between a wide range (from 50 to 300) that depends on several concurring factors and physical quantities that would require a specialized, theoretical, and experimental analysis outside the scopes of the present article. Generally, h_w and h are derived from empirical formulas related to the turbulent flow of fluids (see, for instance, refs 5, 11, and 12 for details); nevertheless, typical values were used here for simplicity.

NUMERIC PREDICTIONS UNDER CONDITIONS OF A CONSTANT TEMPERATURE PROFILE

The determination of the temperature profiles across the cable section does not require inverse-analysis optimization, as described in Figures 2 and 3, but simply the FE solution of Eqs. 1–4.

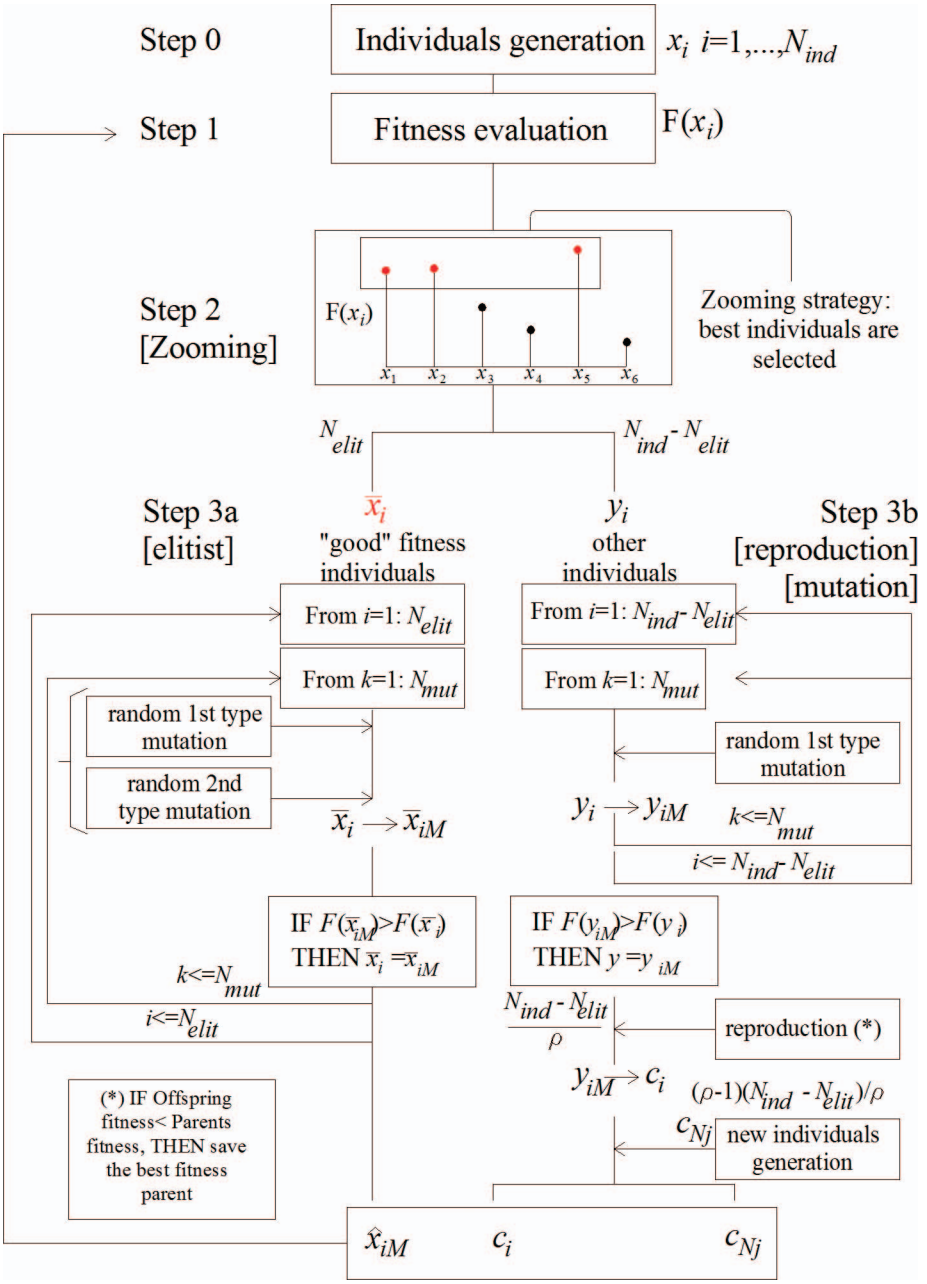

FIG. 3. — Pseudocode of the proposed GA.

Numerically estimated temperature profiles and residual, unreacted peroxide concentrations in the four different vulcanization conditions tested experimentally are shown in Figures 4–7 (for tests 1–4, respectively).

Subfigure panel (a) is the temperature profile at a constant steam temperature (left: 3D view; right: 2D representation at different positions). Subfigure panel (b) is the unreacted peroxide concentration (left: 3D view) or the degree of cross-linking (right: 3D view) deduced from the

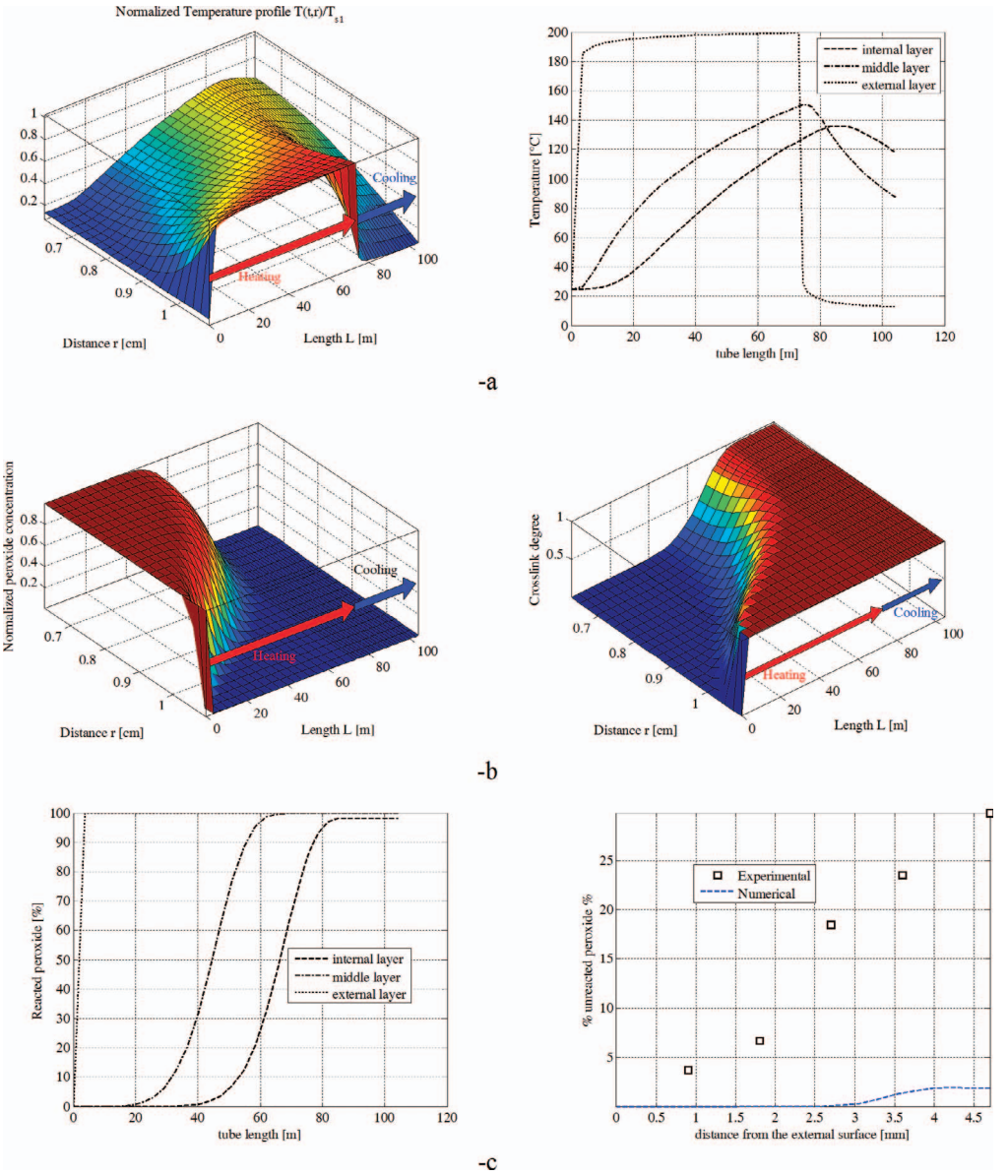

FIG. 4. — Test 1. (a) Temperature profiles at a constant water–steam temperature (left: 3D view; right: 2D representation at different positions). (b) Unreacted and reacted peroxide concentrations (left: unreacted; right: reacted). (c) Evolution of the peroxide reaction at three points along the cable (left) and comparison with experimental data (right).

mathematical kinetic model, and subfigure panel (c) represents the reacted peroxide percentage (left: internal, middle, and external layer; right: comparison with experiments).

The data show a dramatic diversion between the deduced percentage of unreacted peroxide and the experimental evidence, especially for those cases in which a drop in vulcanization temperature was experienced. It can, therefore, be concluded that an inverse analysis would be useful for optimizing and controlling the final level of cable cross-linking.

In addition, it would be interesting to analyze thin sheets in a compression mold experimentally to determine the precise time followed by DSC analysis of the cured material, and consequently, to

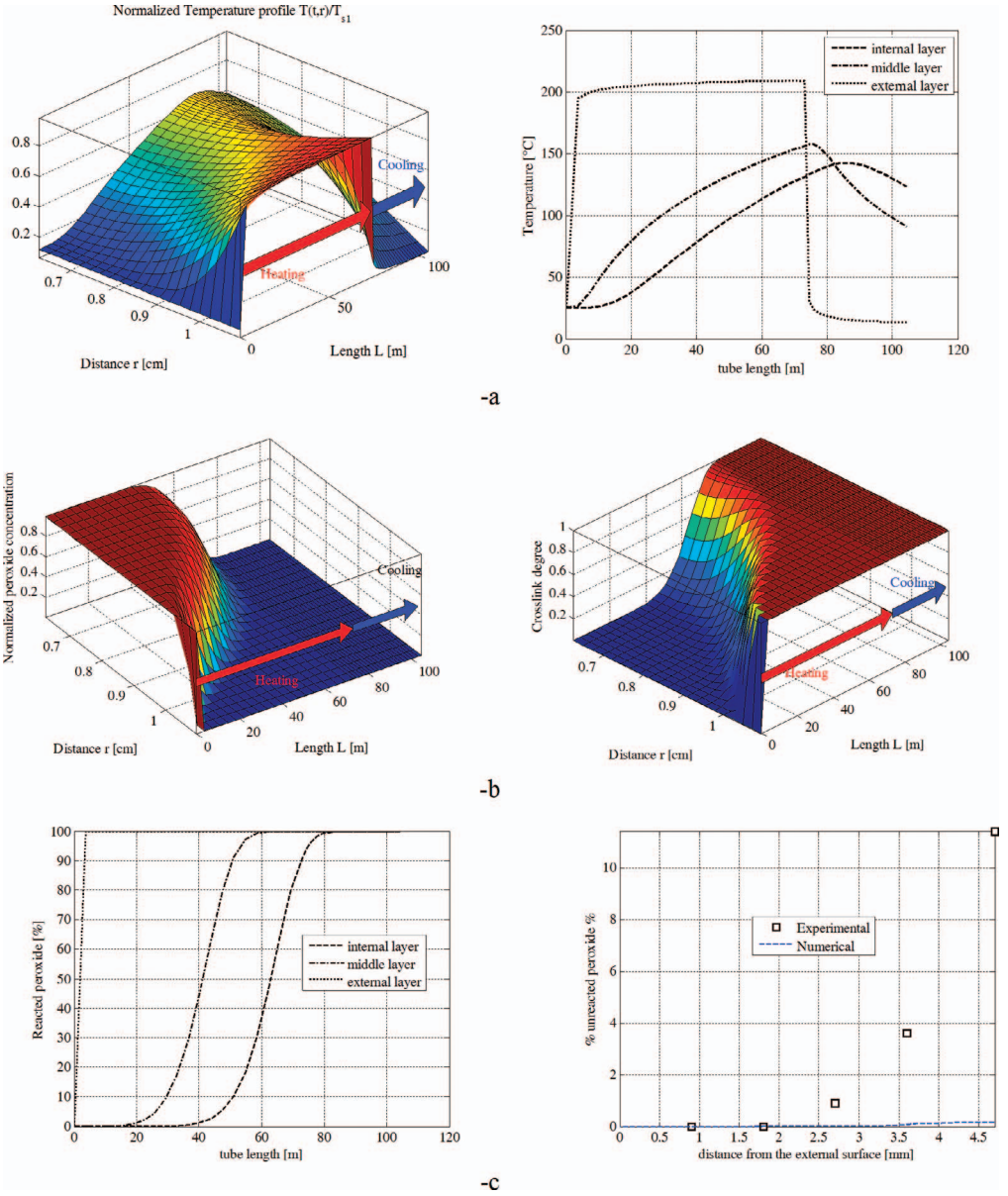

FIG. 5. — Test 2. (a) Temperature profiles at a constant water–steam temperature (left: 3D view; right: 2D representation at different positions). (b) Unreacted and reacted peroxide concentrations (left: unreacted; right: reacted). (c) Evolution of the peroxide reaction at three points along the cable (left) and comparison with experimental data (right).

determine the residual heat of the reaction. Such analyses will be considered in future developments of the research by the authors.

THE GA WITH ADOPTED ZOOMING

When the temperature profile of the steam along the line is not known, inverse analyses are needed to determine the profile that allows the best fit for the final cross-linking level across the cable section (see Figures 2 and 3). Meta-heuristic approaches are particularly useful because the analytical function representing the steam temperature variation along the length is unknown.

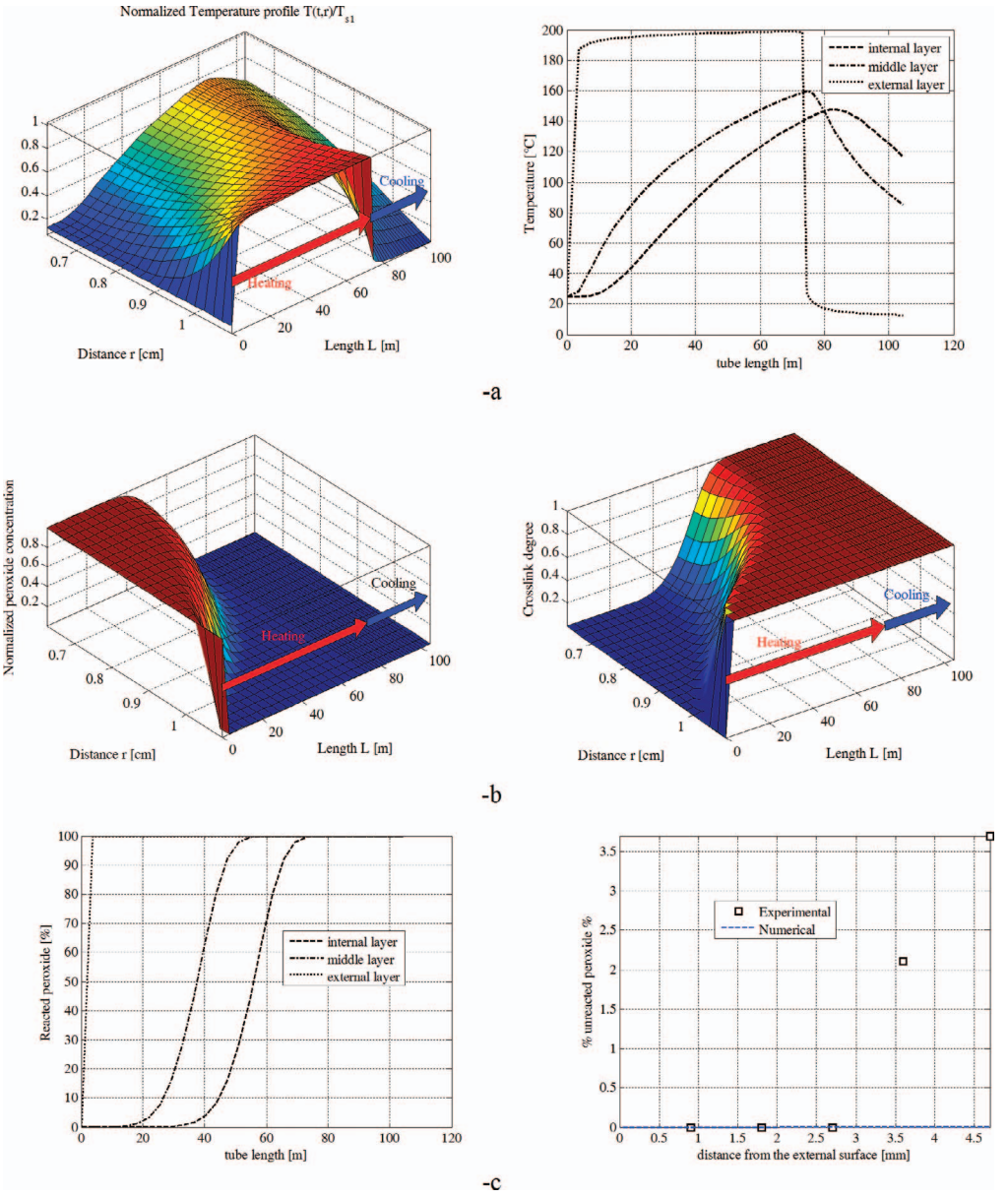

FIG. 6. — Test 3. (a) Temperature profiles at a constant water–steam temperature (left: 3D view; right: 2D representation at different positions). (b) Unreacted and reacted peroxide concentrations (left: unreacted; right: reacted). (c) Evolution of peroxide reaction at three points along the cable (left) and comparison with experimental data (right).

The meta-heuristic approach used is a nonstandard and robust GA, which has already been used in the same context (peroxides) by Milani and Milani[13] and by Milani and Milani[14] and Milani[15] for sulfur. Similar approaches could also be found in refs 16 and 17.

A brief overview describes the peculiar issues of the numeric procedure adopted here. The standard GA adopted in the numerical analysis operates on a population of potential solutions, applying the principle of survival of the fittest, to produce consequential approximated solution.

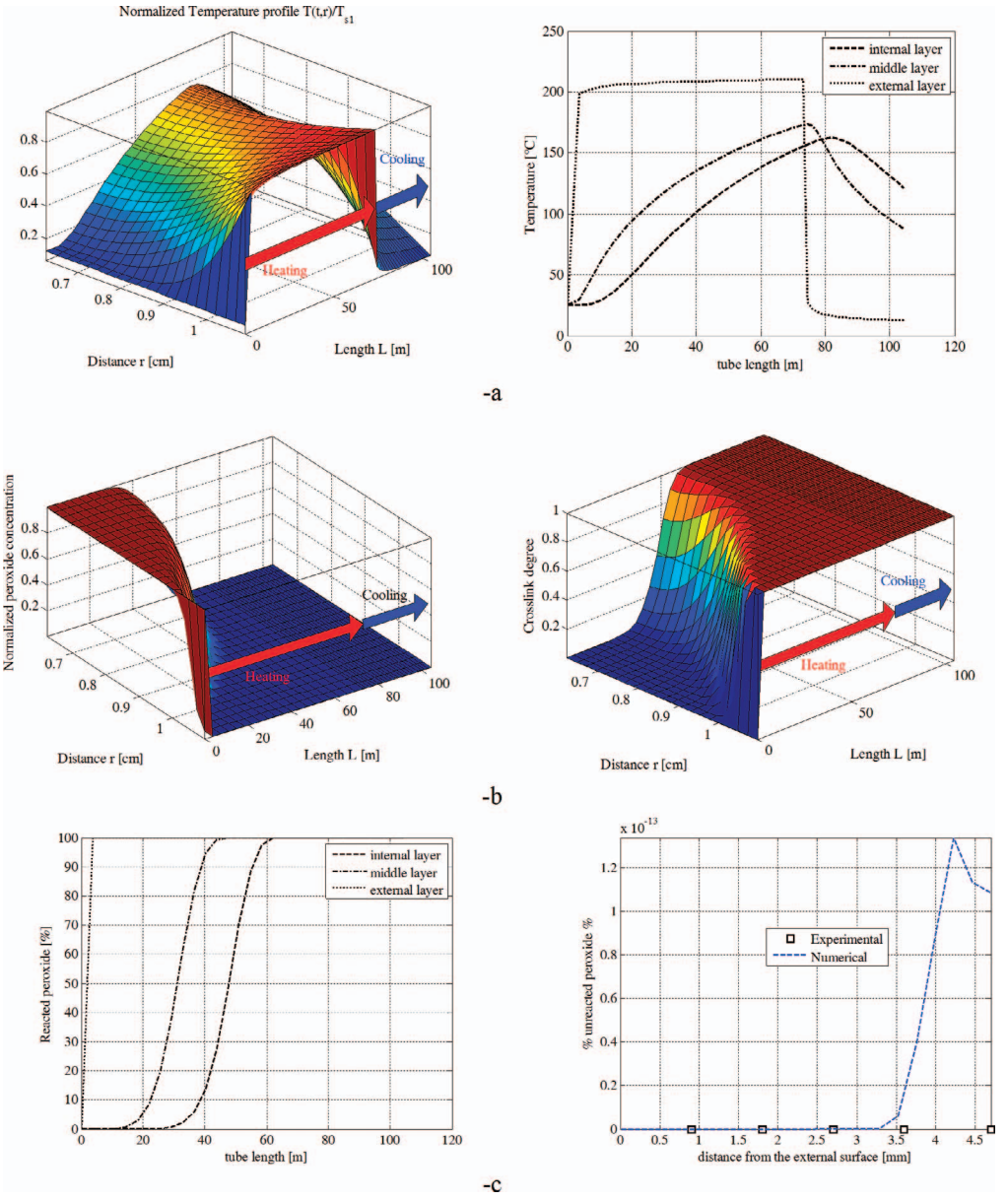

FIG. 7. — Test 4. (a) Temperature profiles at a constant water–steam temperature (left: 3D view; right: 2D representation at different positions). (b) Unreacted and reacted peroxide concentration (left: unreacted; right: reacted). (c) Evolution of the peroxide reaction at three points along the cable (left) and comparison with experimental data (right).

During each solution generation, a new set of approximations is created by selecting individuals according to their level of problem fitness and breeding them together using operators borrowed from natural genetics. This process leads to the evolution of populations of individuals that are better suited to their environment than the individuals they were created from.

The core of the proposed GA is a set of standard (reproduction, crossover, and mutation) and nonstandard (zooming and elitist strategy) genetic procedures. Each individual population is represented by an admissible temperature T_n^i of the steam on a series of control nodes i along the

length of the vulcanization pipe. To simplify calculations, the authors decided to use 10 control nodes, encoding the individuals (real numbers) in binary string. In this way, the genotypes (chromosome values) can be uniquely mapped onto the decision variable (phenotypic) domain. Furthermore, the use of Gray coding is necessary to avoid a hidden representational bias in the conventional binary representation because the Hamming distance between adjacent values is constant.[18,19] The novel characteristic of the proposed GA consists in the division of the population into two subgroups with improvement of the best-fit individuals with zooming.[3,16,20] A graphical representation of the adopted GA code is provided in Figure 3.

An admissible initial population, $\mathbf{x} = \{x_i : i = 1, \ldots, N_{\text{ind}} \mid x_i \text{ admissible}\}$, is randomly generated in step 0 at the first iteration. In step 1, x_i fitness $F(x_i)$ is evaluated, solving a partial differential equation for each layer with a fixed x_i. In step 2, two subgroups are created, namely, $\bar{\mathbf{x}} = \{\bar{x}_i : i = 1, \ldots, N_{\text{elite}} \mid x_i \text{ admissible}\}$ and $\mathbf{y} = \mathbf{x} - \bar{\mathbf{x}} = \{y_i : i = 1, \ldots, N_{\text{ind}} - N_{\text{elite}}\}$. The $\bar{\mathbf{x}}$ is the group of all the individuals with the N_{elite} (user defined) higher fitness values. This step represents the zooming strategy. In step 3a, for each $\bar{x}_i$, a random improvement of the individual (in terms of fitness) is tried, using a mutation operator.[3] The recursive double operation applied randomly N_{mut} times, leads to a new individual generation $\bar{x}_{iM}$, which overwrites the original $\bar{x}_i$ only if its fitness $F(\bar{x}_{iM})$ is greater than $F(\bar{x}_i)$. At the end of the double loop, a new subgroup $\bar{\mathbf{x}}_M = \{\bar{x}_{iM} : i = 1, \ldots, N_{\text{elite}} \mid \bar{x}_{iM} \text{ admissible}\}$ is obtained.

In step 3b, a mutation loop is applied randomly N_{mut} times for each individual y_i with a low fitness value, leading to an improvement of y_i fitness. The new individuals y_{iM} overwrite the original y_i only if their fitness is greater than y_i (the elitist approach). At the end of the double loop, a new subgroup $\mathbf{y}_M = \{y_{iM} : i = 1, \ldots, N_{\text{ind}} - N_{\text{elite}} \mid y_{iM} \text{ admissible}\}$ is obtained. A classic reproduction operator is applied only for individuals of $\mathbf{y}_M$ with high fitness, that is, on $(N_{\text{ind}} - N_{\text{elite}})/\psi$ parents with a user-defined parameter $\psi > 1$, to create a new offspring group $\mathbf{c}$. The remaining $(\psi - 1)[(N_{\text{ind}} - N_{\text{elite}})/\psi]$ individuals are generated ex novo using the step 0 procedure and are catalogued into a $\mathbf{c}_N = \{c_{Nj} : j = 1, \ldots, (N_{\text{ind}} - N_{\text{elite}})/\psi \mid c_{Nj} \text{ admissible}\}$ vector.

Finally, the last population at the ith iteration is collected into $\mathbf{x} = [\bar{\boldsymbol{x}}_M \quad \mathbf{c} \quad \mathbf{c}_N]$, and the procedure is repeated from the beginning.

The use of zooming with an elitist strategy dramatically improves the numeric performance of the algorithm and requires a fraction of the time needed by a standard GA (for instance the GA already implemented in MATLAB).[21]

INVERSE ANALYSIS WITH VARIABLE STEAM TEMPERATURE

The same electric cable subjected to the aforementioned experimental tests may be subjected to a variable steam pressure along the vulcanization pipe. According to the thermodynamic relationship between pressure and temperature in an equilibrium vapor–liquid line (see Figure 8a,b), when the volume is constant and the pressure decreases a consequent decrease in temperature is experienced.

Assuming that the steam water remains at a constant volume (this is unrealistic if the vulcanization tube is airtight), then the empirical relationship $p = (\text{T}/100)^4$ between the pressure p (in bars) and the water temperature T (in °C) may be used to find the pressure measurement and the corresponding temperature. The empirical curve is plotted in Figure 8b for the sake of completeness and allows the monitoring, point by point, of the temperature profile along the vulcanization line by means of a pressure measurement, if the vapor is in equilibrium with the liquid. Such a situation is, however, quite unlikely in practice, and it could be that, for instance, the system has the pressure and temperature identified at point 1. In this case, the entire volume is filled by vapor. From point 1 on, the temperature gets lowers, and the system gets to point 2, or the pressure rises to get to point 3. In either process, it crosses the liquid–vapor equilibrium curve in the direction of condensation from

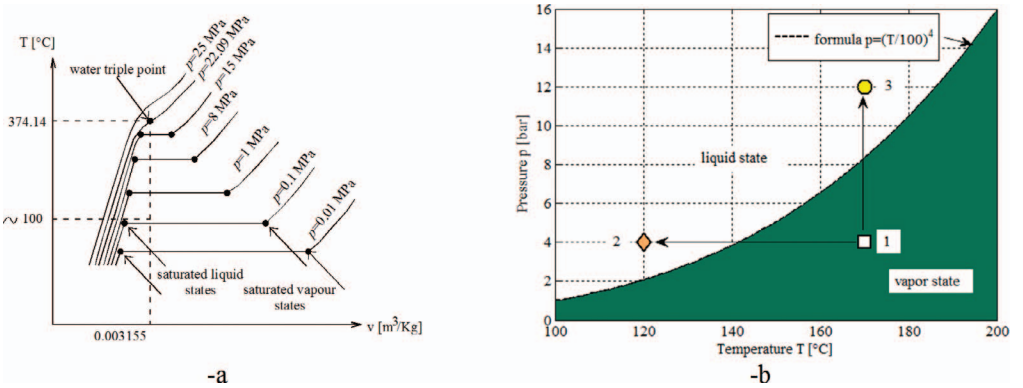

FIG. 8. — Water temperature volume diagram at different pressures (a) and vapor pressure as a function of temperature at the equilibrium (b).

vapor to liquid. It is, therefore, recommended experimentally that the temperature and pressure along the line be monitored with both thermometers and manometers.

The results of the GA approach are summarized in Figures 9–12. Each figure refers to an experimental test: Figure 9 is for test 1, Figure 10 for test 2, Figure 11 for test 3, and Figure 12 for test 4.

Results for the best-fit individual at the last GA iteration are reported, assuming that the individual best fits experimental DSC data.

The temperature profiles with variable steam temperatures are represented in subfigure panels (a) (left: 3D view; right: 2D representation at different positions).

In subfigure panels (b), the unreacted/reacted peroxide concentrations along the cable length and thickness are shown (left: unreacted peroxide concentration 3D view; right: 2D representation of the reacted peroxide at different positions), whereas in subfigure panels (c), the steam temperature profile at the last iteration (the best individual) is depicted, along with a comparison between numerically predicted and DSC reticulation levels.

By comparing the simulation results, the following information is determined:

1. There is a visible drop of temperature in test 1, which fully justifies the unsatisfactory cross-linking level obtained during experimentation. Comparing the results of Figure 9 and the DSC experimental predictions (see part 1, test 1), it is clear that without that drop the cross-linking would be close to optimal.
2. In the second test, there is a regular decrease of the vulcanization temperature along the CV line. The temperature drops in the first and second tests are different, but probably both caused by a systematic loss of pressure along the cable line, which, unfortunately, cannot be controlled by the plant manager.
3. In the third and fourth tests, a loss of temperature is again experienced, but in these cases, they do not affect the cross-linking density.
4. The minimization fitting function is nonconvex and may provide multiple solutions. Similar results may be obtained by assuming a constant steam temperature along the line. This justifies the use of a meta-heuristic approach to deal with problems exhibiting in principle multiple solutions. Standard minimization algorithms based on first-derivative evaluations may potentially fail to find the optimal solution.
5. The convergence and efficiency of the GA approach is demonstrated by the diagram in Figure 13, where the GA performance (in terms of best fit at successive iterations) for one of the performed numeric simulations with variable steam temperature profiles is depicted. Very similar results were seen in all cases.

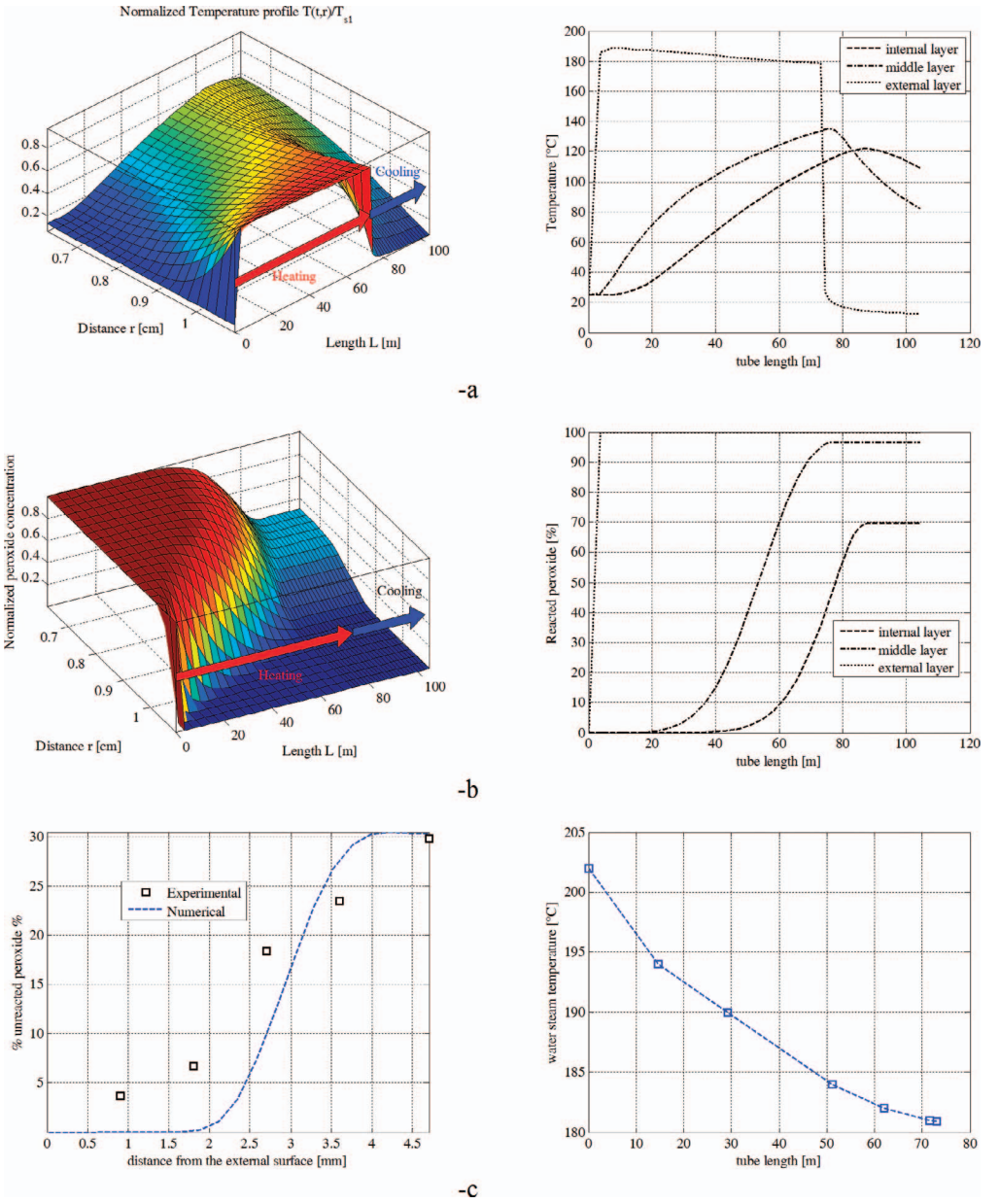

FIG. 9. — Test 1. Best-fit individual at the last iteration. (a) Temperature profiles with variable water–steam temperatures (left: 3D view; right: 2D representation at different positions). (b) Unreacted/reacted peroxide concentration (left: 3D view; right: 2D representation at different positions). (c) Water–steam temperature profile at the last iteration (best individual) (right) and comparison between numerically predicted and DSC reticulation levels (left).

VARIABILITY OF HEAT TRANSFER COEFFICIENTS AND INLET TEMPERATURE

The application of the GA combined with FEs allows us to conclude that the drop in steam temperature along the pipe length may be sufficient to justify the unexpected undervulcanization for certain cure conditions, but these results do not prove conclusively that this is the likely main cause.

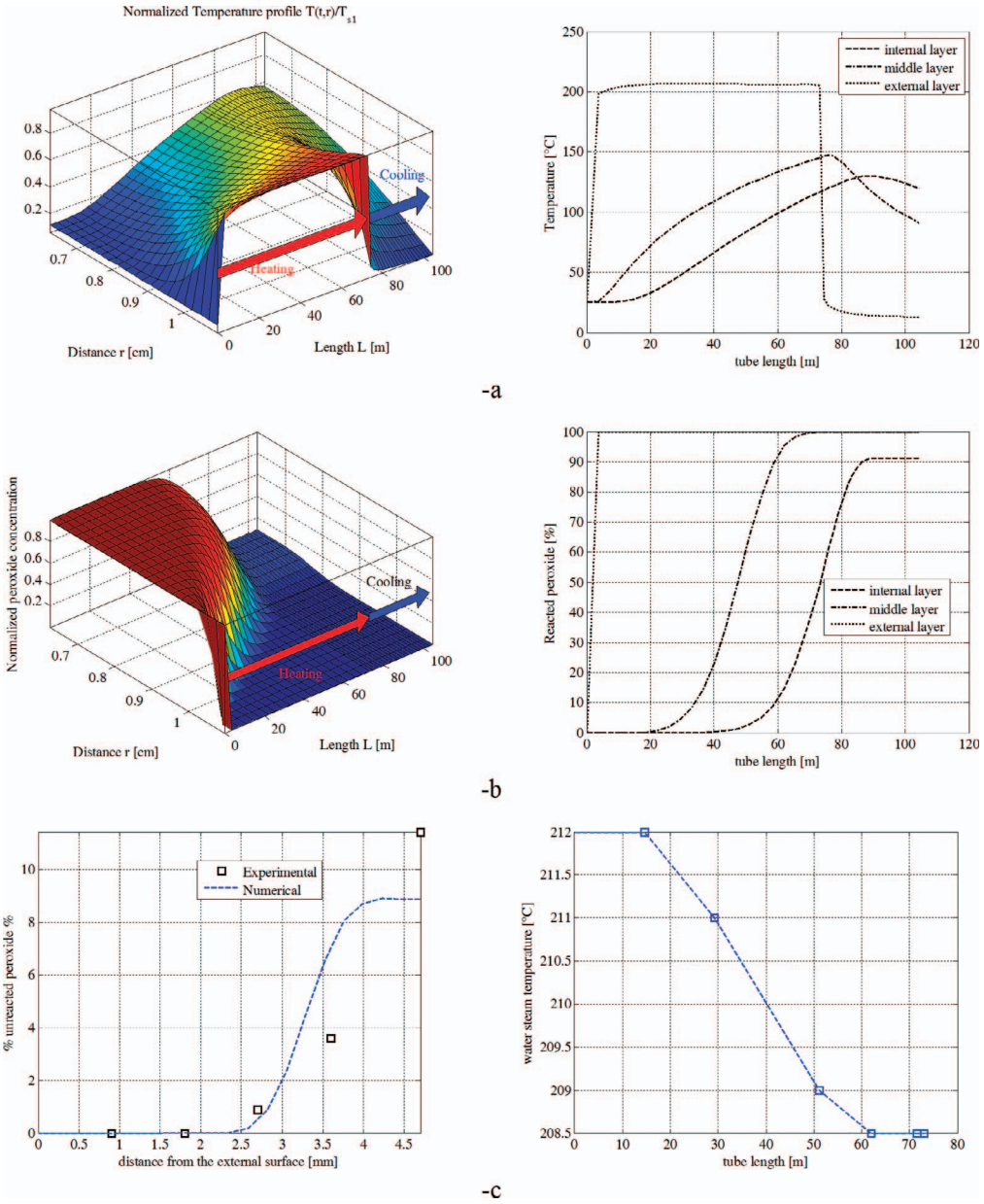

FIG. 10. — Test 2. Best-fit individual at the last iteration. (a) Temperature profiles with variable water–steam temperatures (left: 3D view; right: 2D representation at different positions). (b) Unreacted/reacted peroxide concentration (left: 3D view; right: 2D representation at different positions). (c) Water–steam temperature profile at the last iteration (best individual) (right) and comparison between numerically predicted and DSC reticulation levels (left).

Before assigning the cause of the discrepancy between the computed and experimental states of the cure profiles to an axial temperature decrease, it would be interesting to have an insight into the effect linked to the variation in the different coefficients that were assumed to be constant in the FE computations. In particular, the effect of the values of the presumed heat-transfer coefficients and

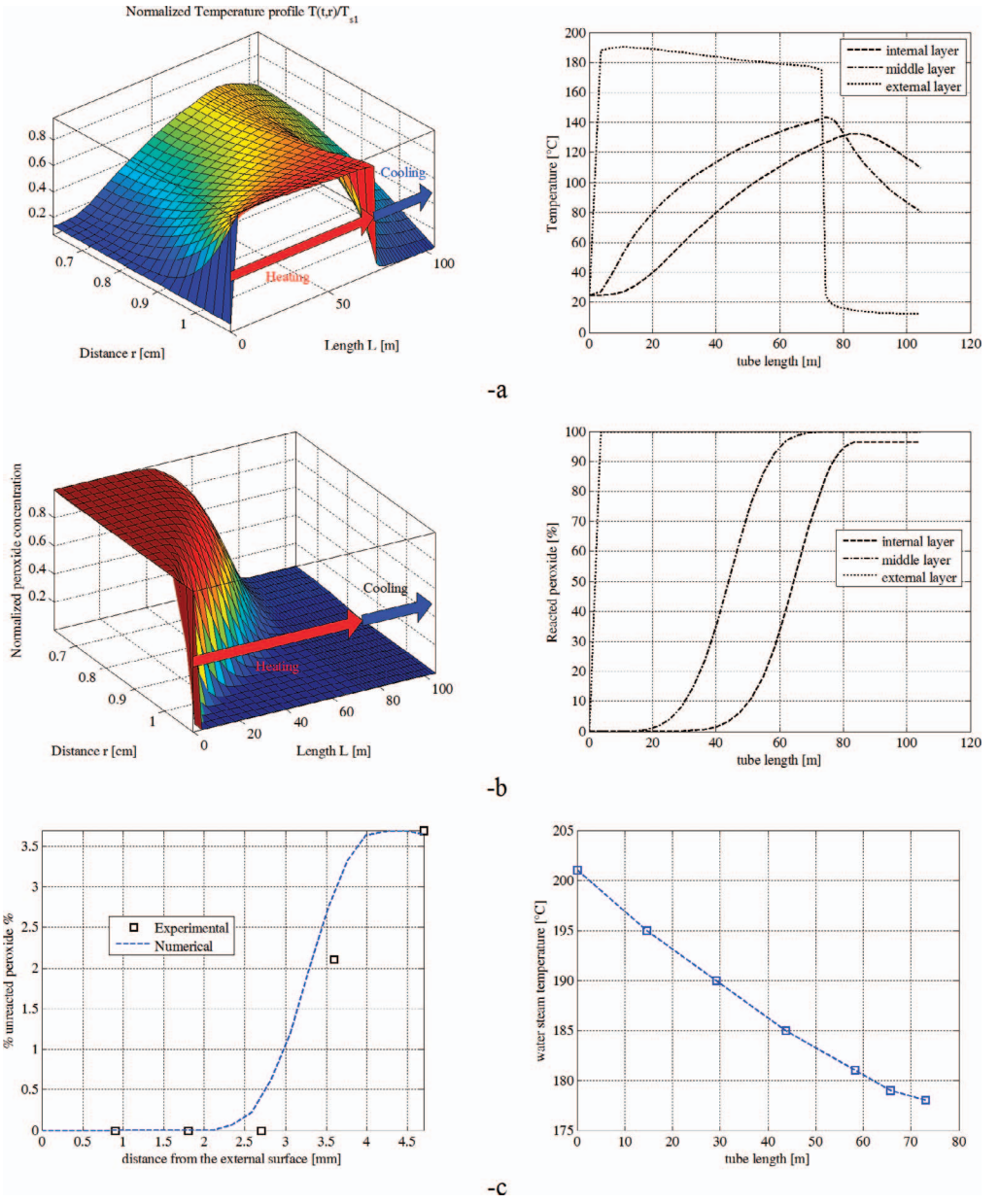

FIG. 11. — Test 3. Best-fit individual at the last iteration. (a) Temperature profiles with variable water–steam temperatures (left: 3D view; right: 2D representation at different positions). (b) Unreacted/reacted peroxide concentration (left: 3D view; right: 2D representation at different positions). (c) Water–steam temperature profile at the last iteration (best individual) (right) and comparison between numerically predicted and DSC reticulation levels (left).

the initial temperature of the insulation on the computed solutions is worth exploring for their agreement with the experimental results.

In addition, the state of the steam in the apparatus seems to indicate that the steam injected into the tube is superheated. If that is the case, then the expression of the relationship between the temperature and the pressure for saturated vapor does not apply. However, if the surface of the

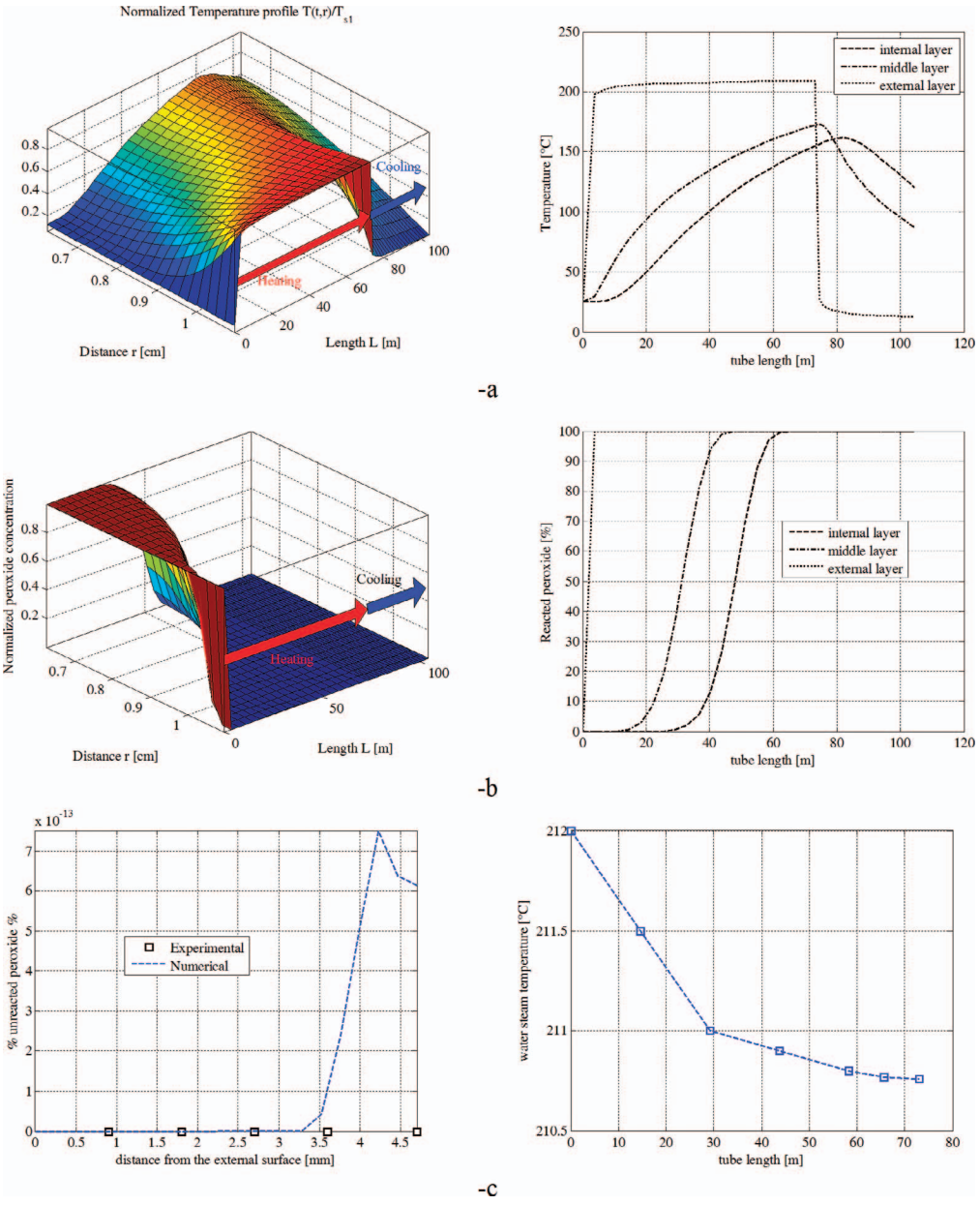

FIG. 12. — Test 4. Best-fit individual at the last iteration. (a) Temperature profiles with variable water–steam temperatures (left: 3D view; right: 2D representation at different positions). (b) Unreacted/reacted peroxide concentration (left: 3D view; right: 2D representation at different positions). (c) Water–steam temperature profile at the last iteration (best individual) (right) and comparison between numerically predicted and DSC reticulation levels (left).

insulation is below the saturation temperature of the steam at the inlet pressure of the tube, then the steam will immediately condense on the surface of the insulation at that temperature. Because the heat-transfer coefficient would be fairly high under these conditions, it is reasonable to assume a constant surface temperature equal to the saturation temperature, which in test 1 is 202 °C for a pressure equal to 16.5 bar. If the surface of the insulation is above that temperature, then the mode of

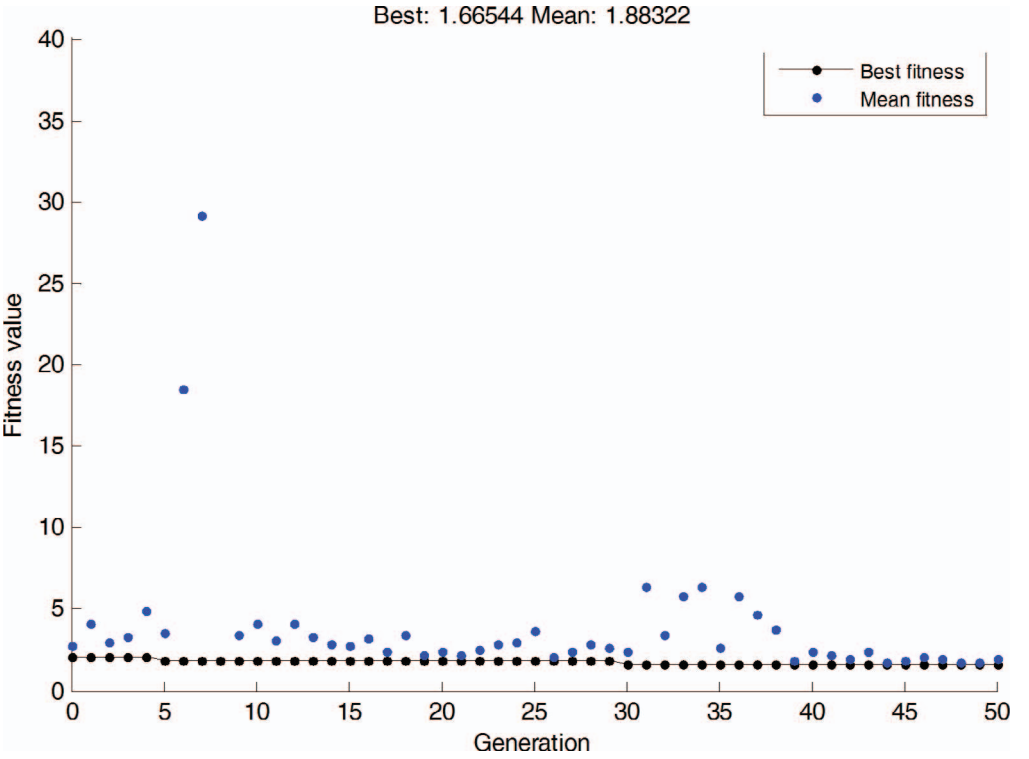

FIG. 13. — GA performance (best fitness at successive iterations) for one of the numeric simulations performed with variable steam–water temperature profiles.

heat transfer is simply forced convection, with the steam temperature decreasing until the saturation temperature is reached.

To account simply for the complex problem of heat exchange, which is unsteady, three additional sets of simulations were performed assuming the following heat-transfer coefficients for the steam: $h = 30$ W/m^2 K, $h = 300$ W/m^2 K, and a variable h along the length of the pipe, with an optimization of the heat-transfer coefficient on experimental data by means of the same GA approach previously used with variable steam temperature. Such lower and upper bounds for the values of h are assumed to be agreement with indications provided in refs 22 and 23.

We assumed steam temperature is constantly equal to $T_1 = 202$ °C, and the total curing time t_c is equal to 5.6 min, that is, the design conditions of test 1 were investigated because the vulcanization level in that case was critical and unexpectedly low. Although we are aware that a realistic numerical simulation should take into account the variability of both T_n and h, such simulations cannot be performed with the GA approach proposed if the relationship between h and T_n is not provided.

However, the evaluation of h (especially as a function of T_n) is a very difficult task, especially when steam condenses and there is a passage between vapor and liquid phases because of unknown heat-unsteady transfer processes.[11,12] In addition, using Newton's law of heat exchange by convection would probably be too simplistic, and the law is only applicable to forced convection, whereas in this case, there is probably an unknown dependence of h on the temperature difference between the steam and rubber surface, as pointed out in refs 11 and 12.

The values adopted for h in the two sets of simulations with constant h values represent the large bounds indicated for steam in forced convection in many handbooks; therefore, such numerical analyses may well approximate upper and lower bounds.

Results obtained assuming constant lower and upper bound values for h are depicted in Figure 14a,b, respectively. The left diagram refers to the temperature profile, whereas plots on the right represent the numerical prediction of the unreacted peroxide along the thickness of the cable, with a comparison with the experimentally determined values.

As shown, when a large value is assumed for h (upper bound), the heat exchange is intuitively favored and the percentage of unreacted peroxide found numerically deviates from the experimental values. The same reasoning applies for an excessively reduced value for h (lower bound). In such a condition, the heat exchange between the rubber surface and the steam becomes slow, and the peroxide reacts at a lower velocity. The resultant percentage of unreacted peroxide is, therefore, greater than that determined experimentally.

Conversely, results obtained assuming that h is variable are in good agreement with the experimental evidence (see Figure 14c). The h profile along the tube length, as determined by the proposed GA, is represented in Figure 15, with a 3D representation of the normalized peroxide concentration (along the thickness and length of the cable). There is a monotonic decrease in h, which assumes very high values at the beginning (superheated condition), which then decreases along the line to typical values for steam-water convection. Although the present simulations are obviously affected by errors induced by the strong simplifications assumed, the results obtained provide interesting information on the steam's physical processes along the line.

When dealing with the initial inlet temperature, the GA simulations were performed assuming a value equal to 25 °C. Such a value is certainly a lower bound and does not take into account the initial heating phase inside the extruder. Here, it is worth noting that to provide realistic numerical simulations inside an extruder is a difficult task, involving 3D FE modeling with coupled thermomechanical approaches. We repeated some of the numerical simulations, adopting a simplified procedure with an increase of the curing temperature from 25 °C to 90 °C in the first 20 m (the length of the extruder) and then starting the simulations. The results of these simulations are reported in Figure 16. As shown, however, the concentration of unreacted peroxide at the end of the simulations (Figure 16b) is very similar to that found with an inlet temperature equal to 25 °C.

CONCLUSIONS

We propose a GA approach to analyze and predict the plant of rubber insulated electric cables. The general methodology was validated with experimental evidence at the end of the production process (see the part 1 article).

The mathematical approach proposed couples the solution of the heat-transmission law in cylindrical coordinates with variable steam temperatures and the application of a genetic algorithm with inverse least-squares data fitting to determine the vulcanization conditions of the samples. The drop in steam temperature depicted by this approach could lead to suboptimal degrees of cross-linking, especially near the core of the insulation, where the heat diffusion is lower.

The optimal degree of cross-linking for a well-defined compound could be achieved by varying the following production parameters: (1) the rate of extrusion, (2) the temperature of the cross-linking, and (3) the ratio between the heating and cooling areas. The formation of areas where the steam becomes liquid water must be avoided.

To support the plant manager through such a difficult task, a numerical tool was developed, and it is now available to be used to set up industrial CV lines.

As shown by the many numerical simulations provided in this article, an accurate experimental estimation of the thermophysical data (the pressure and temperature measurements) of the steam

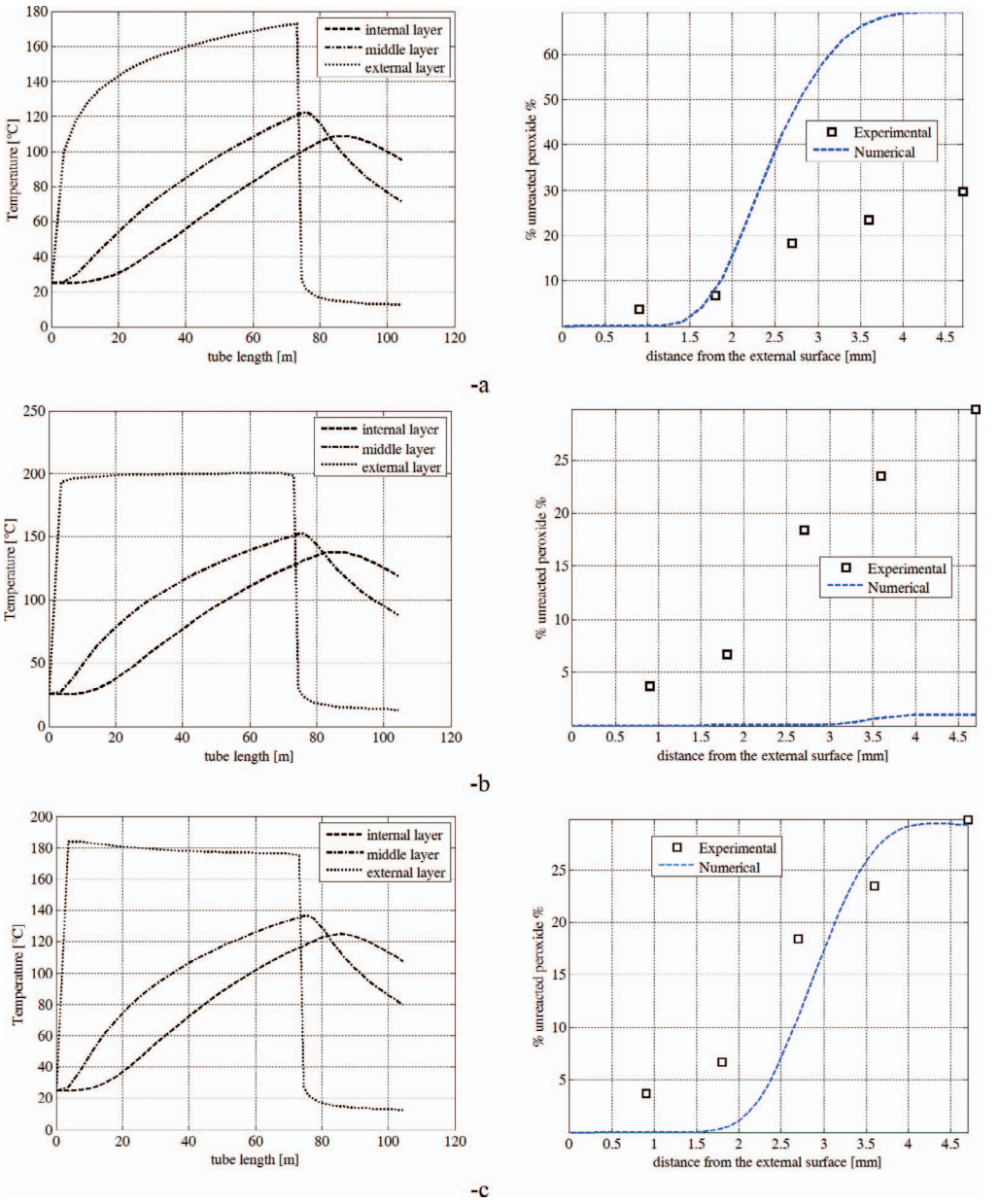

FIG. 14. — Test 1. Results obtained with different values of h. (a) Lower bound for h (left: temperature profile; right: percentage of unreacted peroxide along the thickness at the end of the curing process). (b) Upper bound for h (left: temperature profile; right: percentage of unreacted peroxide along the thickness at the end of the curing process). (c) Variable h (left: temperature profile; right: percentage of unreacted peroxide along the thickness at the end of the curing process).

provided point by point along the pipe length is a key issue in precisely predicting the level of vulcanization for the resulting cured item. Indeed, when dealing with steam vulcanization, the pressure measurements along the pipe are not strictly sufficient to determine the steam temperature because the steam could be superheated. If that were the case, then, the expression of the relationship between the temperature and pressure for saturated vapor does not apply. This is the

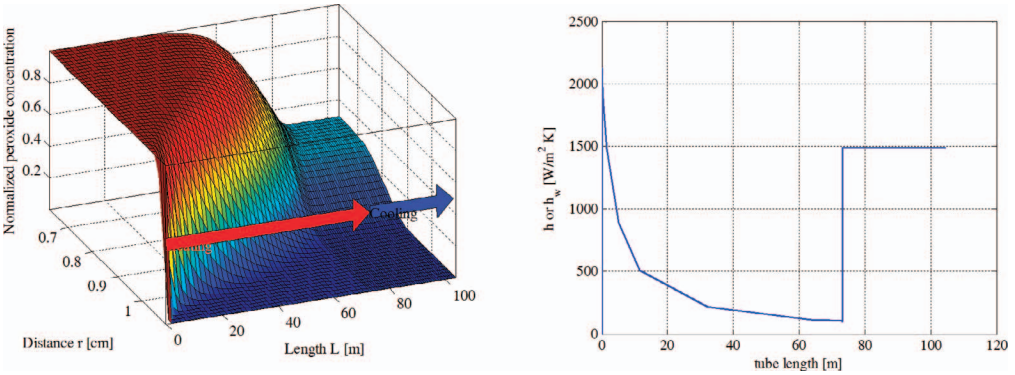

FIG. 15. — Test 1. Results obtained when h was maintained as variable to optimize the GA approach. Left: normalized peroxide concentration along the thickness and the length of the cable. Right: drop in h along the length of the cable.

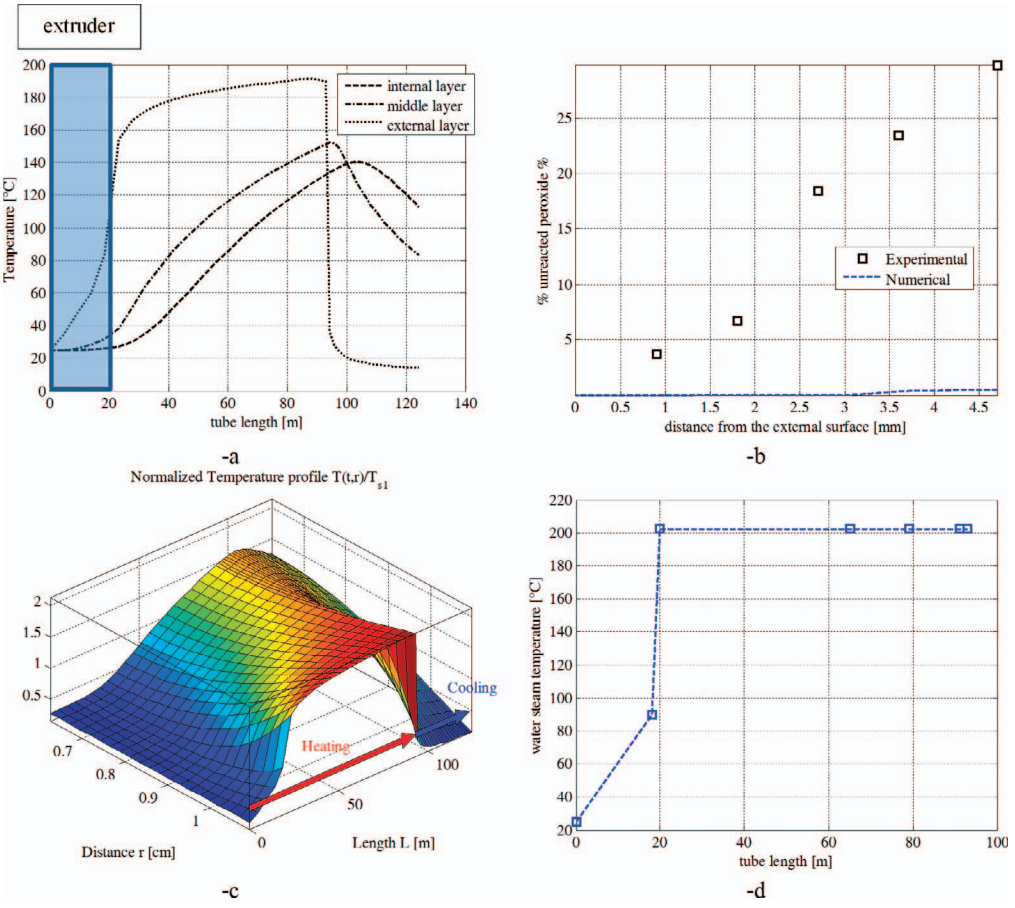

FIG. 16. — Test 1 with the length of the extruder equal to 20 m. Inlet temperature 90 °C, heat transmission coefficient h = 150 W/m^2 K. (a) Temperature profiles along the thickness. (b) Unreacted peroxide percentage. (c) 3D visualization of the temperature along the thickness and length. (d) Water–steam temperature.

reason why pressure measurements should always be coupled with temperature evaluations. If such a monitoring system was at the disposal to the producers, finite elements could accurately predict the level of vulcanization at the end of the production, without the need to provide experimental a posteriori DSC analyses on selected samples. Conversely, the monitoring system coupling finite elements with GAs could be used to optimize the curing apparatus, maximizing the mechanical property output of the insulator, especially in presence of thick items.

REFERENCES

[1]G. A. Prentice and M. C. Williams, RUBBER CHEM. TECHNOL. **53**, 1023 (1980).

[2]M. H. R. Ghoreishy, M. Rafei, and G. Naderi, RUBBER CHEM. TECHNOL. **85**, 576 (2012).

[3]G. Milani and F. Milani, *Comput. Chem. Eng*. **32**, 3198 (2008).

[4]G. Milani and F. Milani, *Polym. Eng. Sci*. **53**, 353 (2013).

[5]V. Kosar and Z. Gomzi, *Thermochim. Acta* **457**, 70 (2007).

[6]V. Kosar, Z. Gomzi, and K. Šintić, *Chem. Eng. Process*. **46**, 83 (2007).

[7]V. L. Lenir, *Polym. Eng. Sci*. **24**, 633 (1984).

[8]G. Milani and F. Milani, *J. Math. Chem*. **51**, 1116 (2013).

[9]G. Milani and F. Milani, *Comput. Chem. Eng*. **43**, 173 (2012).

[10]A. El Labban, P. Mousseau, R. Deterre, and J. L. Bailleul, RUBBER CHEM. TECHNOL. **83**, 331 (2010).

[11]I. Aya and H. Nariai, *Nucl. Eng. Des*. **131**, 17 (1991).

[12]J. H. Lienhard IV, and J. H. Lienhard V, *A Heat Transfer Textbook*, Phlogiston Press, Cambridge, MA, 2011.

[13]G. Milani and F. Milani, *J. Math. Chem*. **47**, 229 (2010).

[14]G. Milani and F. Milani, *J. Math. Chem*. **49**, 1357 (2011).

[15]G. Milani, *J. Math. Chem*. **51**, 465 (2013).

[16]S. L. Kang and W. G. Zong, *Comput. Struct*. **82**, 781 (2004).

[17]E. G. Shopova and N. G. Vaklieva-Bancheva, *Comput. Chem. Eng*. **30**, 1293 (2006).

[18]R. L. Haupt and S. E. Haupt, *Practical Genetic Algorithms*, John Wiley & Sons, Hoboken, NJ, 2004.

[19]R. B. Holstien, "Artificial Genetic Adaptation in Computer Control Systems," Ph.D. Thesis, University of Michigan, 1971.

[20]Young-Doo Kwon, Soon-Bum Kwon, Seung-Bo Jin, and Jae-Yong Kim, *Comput. Struct*. **81**, 1715 (2003).

[21]Matlab, "User's Guide," http://www.matlab.com. Accessed date July 1, 2015.

[22]M. Miccio, "Heat Exchange," Internal report of the University of Salerno [in Italian], http://comet.eng.unipr.it/~miccio/. Accessed date November 3, 2014.

[23]S. A. Gallo, "Industrial Heat Exchange by Steam," Internal Report of the University of Modena [in Italian], https://www.ingmo-old.uimore.it/. Accessed date November 3, 2014.